

Journal of Materials Chemistry B

Accepted Manuscript



This is an *Accepted Manuscript*, which has been through the Royal Society of Chemistry peer review process and has been accepted for publication.

Accepted Manuscripts are published online shortly after acceptance, before technical editing, formatting and proof reading. Using this free service, authors can make their results available to the community, in citable form, before we publish the edited article. We will replace this *Accepted Manuscript* with the edited and formatted *Advance Article* as soon as it is available.

You can find more information about *Accepted Manuscripts* in the [Information for Authors](#).

Please note that technical editing may introduce minor changes to the text and/or graphics, which may alter content. The journal's standard [Terms & Conditions](#) and the [Ethical guidelines](#) still apply. In no event shall the Royal Society of Chemistry be held responsible for any errors or omissions in this *Accepted Manuscript* or any consequences arising from the use of any information it contains.

Cite this: DOI: 10.1039/c0xx00000x

www.rsc.org/xxxxxx

PAPER

Size dependent biological profiles of PEGylated gold nanorods

Francesca Tatini^a, Ida Landini^b, Federica Scaletti^c, Lara Massai^c, Sonia Centi^d, Fulvio Ratto,^{*a} Stefania Nobili^b, Giovanni Romano^d, Franco Fusi^d, Luigi Messori^c, Enrico Mini^b, Roberto Pini^a

Received (in XXX, XXX) Xth XXXXXXXXX 20XX, Accepted Xth XXXXXXXXX 20XX

DOI: 10.1039/b000000x

The perspective to introduce plasmonic particles for applications in biomedical optics is receiving much interest. However, their translation into clinical practices is delayed by factors that include a poor definition of their biological interactions. Here, we describe the preparation and the biological profiles of gold nanorods belonging to five different size classes with average effective radii between ~ 5 and 20 nm and coated with polyethylene glycol (PEG). All these particles exhibit decent stability in the presence of representative proteins, low cytotoxicity and satisfactory compatibility with an intravenous administration, in terms of their interference with blood tissue. However, the suspension begins to become unstable after a few days of exposure to blood proteins. Moreover, the cytotoxicity is a little worse for smaller particles, probably because their purification is more critical, while undesirable interactions with the mononuclear phagocyte system are minimal in an intermediate range of sizes. Overall, these findings hold implications of practical relevance and suggest that PEGylated gold nanorods may be a versatile platform for a variety of biomedical applications.

Introduction

The cellular applications of plasmonic particles in the context of biomedical optics, ranging from imaging and diagnostics to therapeutics, have received considerable attention over recent years.¹⁻⁵ With actual perspectives to reach the clinical arena, the need for well-characterized and biocompatible particles is becoming urgent. However, in spite of an increasing number of studies, the available data in the scientific literature remain fragmented and heterogeneous.^{6,7}

Among the various plasmonic particles, so-called gold nanorods (GNRs) are attracting particular interest because of their peculiar optical properties, extreme efficiency and stability of photothermal conversion⁸ and biochemical versatility. Their optical absorbance exhibits two intense resonances that correspond to orthogonal modes of plasmonic oscillations, i.e. a transversal mode in the green region and a longitudinal mode in a range of frequencies that may be tuned in the far red-near infrared window (650-1000 nm) of principal interest in biomedical optics. The wavelength of this resonance depends on the particle shape and in particular the aspect ratio (i.e. length divided by diameter, AR), with the particle size playing a secondary role.^{9,10} Other factors of impact on the frequency of both transversal and longitudinal bands are the refractive index of the environment and particle aggregation.¹¹ All these features make GNRs ideal contrast agents and sensitizers for applications such as the photoacoustic imaging and the optical hyperthermia of cancer.

Crucial features of GNRs include their coating, shape and size. The kind of coating is critical to modulate their interface with the biological systems, enable to bind functional moieties such as

ligands and govern the colloidal stability in culture media and body fluids. Polyethylene glycol (PEG) is perceived as the coating of choice because of its biocompatibility,¹²⁻¹⁴ ability to avoid the detection from macrophages, readiness of biochemical modification and steric hindrance against particle aggregation. As it was mentioned, the choice of particle shape follows from the need for specific spectral features.

Therefore, particle size remains the principal variable to play with. Particle size may modulate critical parameters such as: the cellular penetration,^{15,16} the intracellular localization,¹⁷ the biodistribution,¹⁸ features that depend on specific surface area, including the rate of interaction with proteins, residual toxicity of contaminants or load of ligands,¹⁷ the ratio of optical absorption to scattering,¹⁰ the efficiency and stability of photothermal conversion and the optical and thermal hotspot distribution.¹⁹ We recall that, for individual GNRs, the light extinction cross sections roughly scale with the particle volumes.^{8,10} Therefore, in order to maintain the same optical absorbance, one should compare samples containing the same gold molarity, rather than e.g. the same particle density by number.

Here, we present an extensive survey on the characterization, stability, toxicity and cellular uptake of PEGylated GNRs (PEG-GNRs) of five different size classes. A critical requirement for biomedical applications of GNRs is their colloidal stability in physiological buffers. Previous studies showed that gold nanoparticles exposed to biological fluids may become coated with proteins,^{20,21} which may modify their conformation, thus causing a loss of their biological activity,²² elicit an altered immune response and modulate their biodistribution and cellular uptake. Here, we address the effect of particle size on the stability of PEG-GNRs in biological buffers and look at their interactions

with significant proteins, such as the lysozyme, cytochrome c (cyt c) and bovine serum albumin (BSA).

The correlation between size and toxicity of gold nanoparticles of various shapes has been investigated in a few cases with alternate results.^{13,18,23-27} While as-synthesized cetrimonium-stabilized GNRs impart significant cellular damage, PEG-GNRs display little cytotoxicity.^{14,28,29} This cytotoxicity may persist from the retention of contaminants used in the synthesis, such as cetrimonium and silver ions, which may explain the correlation between particle surface area and cellular damage^{13,30} and project a stronger toxicity for smaller particles.^{18,24,31} To our knowledge, the effect of size on the cytotoxicity and cellular uptake of PEG-GNRs has never been reported before, which requires a careful examination of multiple parameters including cell proliferation, viability, membrane integrity and blood compatibility. Moreover, in order to avoid a possible bias that may affect existing data⁷ due to the use of HeLa cells with their anomalous phenotype, we resort to a battery of cellular models. Finally, the size of PEG-GNRs may affect their cellular uptake by nonspecific interactions, which is another critical issue in view of biomedical applications. Although the available literature is inconclusive,⁶ particle size was found to modulate their cellular uptake and determine different mechanisms of internalization.^{6,20} Here, we scan all these issues in a range of particle concentrations of common use in preclinical trials for therapeutic applications in rodents, i.e. in the order of 10 mg Au / Kg tissue, or 50 μ M Au.³²⁻³⁵

Methods

Chemicals

Sodium borohydride, cetrimonium bromide, chloroauric acid, silver nitrate, ascorbic acid, alpha methoxy omega mercapto polyethylene glycol (MW 5000), polysorbate 20, sulforhodamine B and all chemicals for the various buffer solutions were obtained from Sigma Aldrich and used as received. Cell culture media (RPMI1640, DMEM and F12), fetal calf serum and antibiotics (penicillin, streptomycin) were purchased from Gibco. The water for particle synthesis was ultrapure.

Synthesis of PEGylated gold nanorods

Gold nanorods were synthesised at 25°C. A seed suspension was prepared by rapid injection of ice-cold 10 mM aqueous sodium borohydride into a solution containing 100 mM cetrimonium bromide and 240 μ M chloroauric acid until a final concentration of 560 μ M sodium borohydride. This suspension was left under vigorous agitation for 10 min and then at rest for another 2 hours before rapid addition into a growth solution in different amounts. Meanwhile 500 ml growth solution were prepared with 100 mM cetrimonium bromide, 470 μ M chloroauric acid, 92 μ M silver nitrate and 520 μ M ascorbic acid. This solution was divided into five aliquots with a volume of 100 ml each, before injection of 1.8 (particle sample 1/9), 0.59 (1/3), 0.20 (1), 0.066 (3) or 0.022 ml (9) seed suspension. After 24 hours, 100 mM aqueous ascorbic acid was added until a total content of 710 μ M ascorbic acid, which served to complete the metal reduction.^{36,37}

After two cycles of centrifugation and decantation, particles were transferred at a rate of 1.9 mM Au into an acetate buffer at pH 5 containing 500 μ M cetrimonium bromide and 50 μ M alpha

methoxy omega mercapto PEG (MW 5000). The PEGylation was left to develop at 37°C for two hours, before centrifugation, decantation and resuspension in 1% (v/v) aqueous polysorbate 20. This suspension was left at rest for 2 hours at 37°C, in an attempt to extract possible contaminants. Finally, PEG-GNRs were transferred at a rate of 4.0 mM Au into sterile PBS after purification by four cycles of centrifugation and decantation with a dead volume ratio of \sim 1 / 200.

Cell growth and viability

All cellular lines were maintained under standard conditions as described in the Electronic Supplementary Information (ESI). For cell growth and viability studies, cells were inoculated into 96-well microplates. After 24 h, the medium was replaced with fresh medium containing PEG-GNRs. The inhibition of cell growth was studied on SKOV3, IGROV-1, A2780/S and HeLa cells, according to the sulforhodamine B (SRB) assay described by Skehan *et al.*³⁸ SRB assay was performed after 72 and 168 h of incubation with PEG-GNRs. For cell viability evaluation, the 3-(4,5-Dimethylthiazol-2-yl)-2,5-diphenyltetrazolium bromide (MTT)³⁹ test was conducted after 24 h of exposure to PEG-GNRs. More detail for cell growth and viability studies is given in the ESI.

Cell membrane permeability

To assess membrane integrity disruption, after cell inoculation, the microtiter plates were incubated under standard culture conditions for 24 h and then treated with 2.0 μ M calcein-AM for 20 min. Then, the medium was replaced with fresh medium containing PEG-GNRs with 300 μ M Au for 3 h. After treatment, cells were extensively washed with PBS and imaged using a Leica DMI3000B inverted microscope.

Haemolysis

For the evaluation of haemolysis, informed signed consent was obtained and human whole blood was collected from healthy volunteers. EDTA (1.8 mg/ml)-containing test tubes were used to collect the whole blood, which was centrifuged at 3000 rpm for 20 min. The buffy coat was collected, washed and diluted with normal saline to a 50% hematocrit. 100 μ l of these samples were added to 3 ml of normal saline (negative control), ultrapure water (positive control) and PEG-GNRs suspensions in PBS at different concentrations. All samples were incubated at 37°C for 1 h and haemolysis was stopped by the addition of 50 μ l of 2.5% glutaraldehyde prior to centrifugation at 3000 rpm for 15 min. Supernatants were collected in 96-well microplates and their absorbance at 405 nm was measured using an automated plate reader.

Stability of PEGylated gold nanorods

Spectrophotometric studies were performed by a Jasco V-560 spectrophotometer. Optical extinction spectra were recorded after dilution of PEG-GNRs either in PBS or RPMI at physiological pH. The final gold concentration in the various suspensions was 100 μ M. Spectra of PEG-GNRs in PBS were recorded before and after addition of 10 μ M BSA, lysozyme and cyt c. All spectra were collected over 168 h both at room temperature and at 37°C. In order to achieve additional evidence of possible interactions between PEG-GNRs and proteins in a representative case, 10 μ M

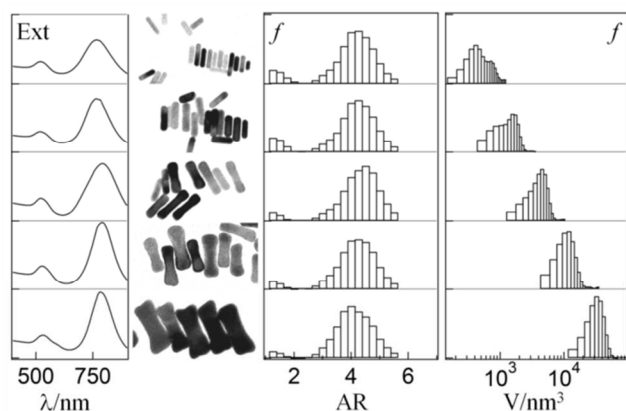


Fig. 1 Light extinction spectra, representative (170×100) nm² TEM micrographs, volumetric distributions of particle aspect ratios and volumes of samples GNRs 1/9, 1/3, 1, 3 and 9 from top to bottom.

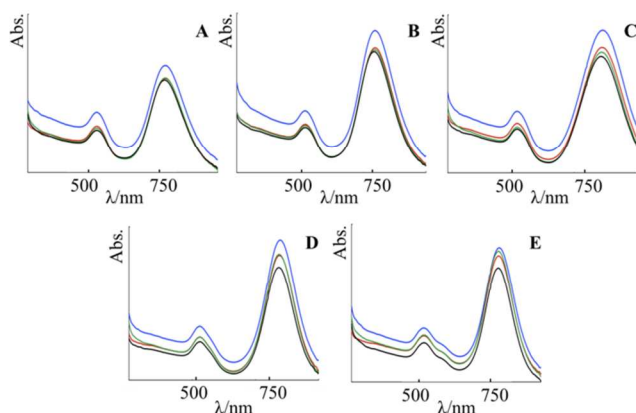


Fig. 2 Light extinction spectra of PEG-GNRs of different average size in PBS containing BSA A) GNRs 1/9; B) 1/3; C) 1; D) 3; E) 9. The figure shows spectra recorded at time zero (black line) and after 1h (green line), 24h (red line) and 168h (blue line).

10 cyt c was incubated with 100 μ M Au PEG-GNRs 1 in PBS at 37°C. After 24 hours, the sample was separated by centrifugation at 10000 rpm for 13 min, the supernatant was collected and the pellet was suspended in PBS. Both components were analyzed by a Varian Cary 50 Bio UV/Vis spectrophotometer.

15 Particle composition and cellular uptake by elemental analysis

The determination of gold and silver concentrations in the particles was performed in triplicate by a Varian 720-ES Inductively Coupled Plasma Atomic Emission Spectrometer (ICP-AES).⁴⁰ Before analysis, 10 μ l suspension of PEG-GNRs in PBS were digested in PE vials by heating at 80°C for 24 hours with 1 ml aqua regia (HCl suprapure grade and HNO₃ sub-boiled in 3:1 ratio). HeLa cells and J774a.1 cells that had been exposed to PEG-GNRs were digested by heating at 80°C for 24 hours with 25 1 ml aqua regia and 100 μ l H₂O₂ suprapure grade. After digestion, samples were diluted to 5 ml with ultrapure water, spiked with 4 ppm Ge used as internal standard and analyzed. Wavelengths used for Ag, Au and Ge were 328.068, 242.794 and 209.426 nm, respectively. Between samples, a rinse solution 30 containing 2% v/v HNO₃ was used.

Cellular uptake by electron microscopy

J774a.1 cells were seeded onto transwell membranes and treated overnight with PEG-GNRs. Cells were then washed and fixed with paraformaldehyde (3,6%, 5 min at room temperature).
35 Samples were washed with fresh PBS and membranes were cut in triangles, post-fixed in 1% osmium tetroxide in PBS at 4°C for 2 h, washed again, dehydrated in a graded series of ethanol at room temperature and incubated in propylene oxide (twice, 30 min each time). Samples were then incubated in 1:1 mixture of
40 propylene oxide and Spurr resin for 24 h at room temperature, next in 1:2 mixture for 1 h at room temperature and finally in pure resin for 1 h at room temperature, 1 h at 45°C and 24 h at 70°C. After sectioning and staining with uranyl acetate for 1 h at room temperature, slices were washed and inspected with a
45 Philips CM12 transmission electron microscope.

Results

Size and shape of gold nanorods

In order to be as representative as possible, PEG-GNRs were prepared by usual protocols with minimal modifications to tune
50 their size statistics. In particular, GNRs were synthesized by the common seed-mediated approach,^{36,41} where particle growth is triggered by the injection of gold nuclei in a growth solution and develops without additional nucleation.^{36,37} The initial seed density equals the final particle density and so dictates the
55 average particle size, because the ions in the growth solution are shared in either of a larger number of smaller particles or a smaller number of larger particles. Instead the typical particle AR exhibits little dependence on the initial seed density. Here, these notions were exploited to modulate the average particle size at
60 comparable shape statistics.

Figure 1 displays a spectroscopic and microscopic analysis of samples that were prepared by implementation of five seed densities in different aliquots of a growth solution from a common batch (before PEGylation). From sample to sample, the
65 experimental spectra are consistent in terms of peak intensities and positions, which reflect their sameness of gold molarity^{19,37,42} and typical particle shapes, respectively. The transmission electron micrographs corroborate our predictions on the trends of particle volumes and AR with the seed density. The spread of
70 these parameters is in line with that of most academic labs.^{8,36} The volumetric distributions of particle AR are consistent from sample to sample, despite subtle modifications of particle shapes, such as lesser quasi spherical byproducts and more dogbone profiles^{36,43} at lower seed densities. Instead, typical particle
75 volumes scale well with the inverse of the seed density. The average particle effective radii are (19.4 ± 0.4), (13.5 ± 0.3), (9.8 ± 0.2), (6.8 ± 0.2) or (4.8 ± 0.1) nm. We note that the overlap between the volumetric distributions of particle volumes of every second sample is rather negligible.

80 After synthesis, GNRs were PEGylated by standard methods for gold nanoparticles and substrates. By the use of dynamic light scattering, we found that the hydrodynamic thickness of the PEG shells in PBS was about 13 – 18 nm for all samples, which suggests a so-called brush configuration and a density in the order
85 of 0.8 PEG strands per nm².⁴⁴ Purification from contaminants was pursued by extraction in a common surfactant such as polysorbate 20 and five cycles of centrifugation and decantation. Additional

Cite this: DOI: 10.1039/c0xx00000x

www.rsc.org/xxxxxx

PAPER

Table 1 Inhibitory effect of 5 different suspensions of PEG-GNRs on cell growth of HeLa, A2780/S, SKOV3 and IGROV-1 cell lines after 72 and 168 h exposure.

PEG-GNRs	IC ₅₀ ± SD (μM) ^a							
	HeLa		A2780/S		SKOV3		IGROV-1	
	72 h	168 h	72 h	168 h	72 h	168 h	72 h	168 h
9	> 100	> 100	> 100	> 100	> 100	> 100	> 100	41.0 ± 17.4
3	> 100	> 100	> 100	> 100	> 100	> 100	> 100	18.3 ± 1.4
1	> 100	> 100	> 100	> 100	> 100	> 100	> 100	10.3 ± 4.3
1/3	> 100	> 100	> 100	> 100	> 100	77.5 ± 3.0	> 100	13.5 ± 5.1
1/9	> 100	> 100	> 100	> 100	> 100	53.7 ± 4.6	> 100	18.9 ± 10.8

^a IC₅₀ is defined as the concentration of drug required to inhibit cell growth by 50%; SD, standard deviation; data represent the mean of three independent experiments each performed in triplicate.

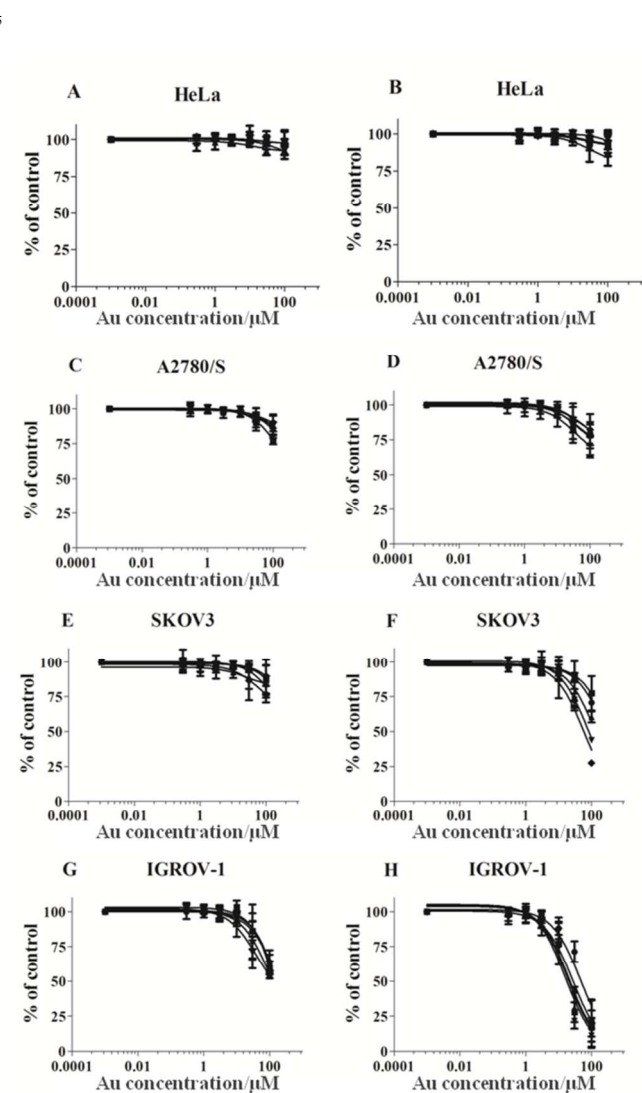


Fig. 3 Cytotoxic effects of 5 different suspensions of PEG-GNRs on cell growth of HeLa, A2780/S, SKOV3 and IGROV-1 cell lines after 72 h (panels A, C, E, G) and 168 h (panels B, D, F, H) exposure. The figure shows values for GNRs 9 (●), 3 (■), 1 (▲), 1/3 (▼), 1/9 (◆).

details on sample preparation are given under subsection Methods.

Our variety of particle sizes covers the range of principal interest for biomedical applications, smaller particles beginning to display poor plasmonic oscillations⁴⁵ and larger particles becoming problematic for blood circulation.⁴⁶ Hereafter, our samples will be labelled with the numbers 9, 3, 1, 1/3, 1/9, which indicate their relative average particle volumes with respect to sample 1. The latter corresponds to a standard size of ~ 41 nm average length per ~ 10 nm average diameter.

Stability of PEGylated gold nanorods

PEG-GNRs proved to be stable in the most common buffers for cell biology and in the presence of representative proteins. In order to understand the stability of PEG-GNRs in the presence of representative biological components, we monitored possible variations of their plasmonic bands at ~ 520 and ~ 780 nm, which display high sensitivity to particle aggregation,¹¹ protein adsorption and charge injection.^{47,48}

PEG-GNRs were diluted in a reference PBS buffer at physiological pH to a final concentration of 100 μM Au and their optical extinction was monitored over one week at 25°C. No noticeable changes occurred over the entire observation period, which implies the absence of aggregation or sedimentation. Subsequently, we tested the stability of the various PEG-GNRs in the presence of relatively large concentrations of representative proteins. Experiments were performed at 37°C, in an attempt to represent physiological conditions. Three different proteins were chosen for these tests, namely BSA (Figure 2), lysozyme and cyt c (Figures S1 and S2 of the ESI). The choice of these proteins was guided by their importance, globular structure, stability, solubility and availability. Their addition up to a final concentration of 10 μM did not significantly affect the plasmonic bands of all PEG-GNRs. Only minor shifts were noticed around 780 nm in a few cases. The onset of partial flocculation and sedimentation led to a modest decrease in optical density over one week. The case of cyt c is particularly informative, as this protein exhibits an intense Soret band around 400 nm, arising from its heme cofactor. This feature allowed us to simultaneously monitor both the proteins and the particles. No significant changes were observed right after mixing nor afterward, which

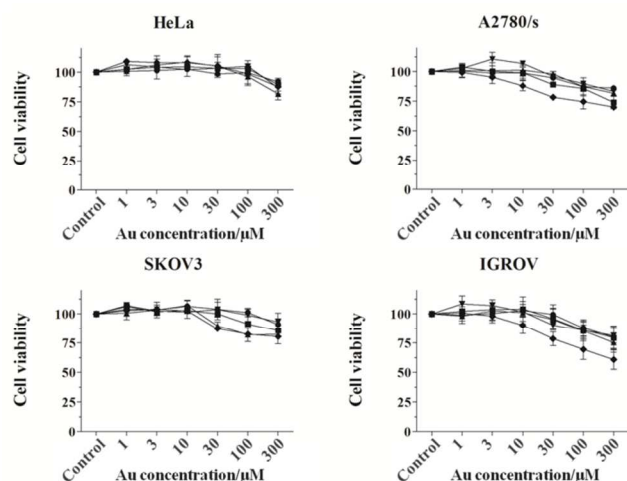


Fig. 4 MTT reduction test for cell viability on HeLa, A2780/S, SKOV3 and IGROV-1 cell lines after 24 h exposure to PEG-GNRs. Cell viability is expressed as percent of MTT reduction in treated cells with respect to control cells. Reported data represents the mean \pm standard deviation of three independent experiments. The figure shows values for GNRs 9 (●), 3 (■), 1 (▲), 1/3 (▼), 1/9 (◆).

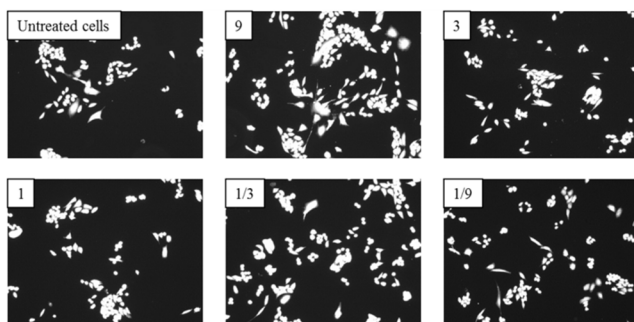


Fig. 5 Calcein fluorescence in untreated A2780/S cells and after treatment with PEG-GNRs of different average size.

implies a substantial weakness of possible interactions. Direct evidence of this weakness comes from the possibility to readily separate these species by centrifugation. The residual amount of cyt c adsorbed on PEG-GNRs turned out to be negligible, as it is shown in Figure S3 of the ESI.

We also analyzed the effects of an addition of RPMI medium (Figure S4). For all PEG-GNRs, there occurred significant and progressive red-shifts of the main bands at 780 nm. This process is relatively slow and reaches completion in a few days. In agreement with previous reports, red-shifts imply changes in the local environment of the PEG-GNRs.^{47,48} We hypothesize that this effect may follow from the interplay of partial PEG substitution and selective adsorption of different components in a complex environment such as RPMI.⁴⁹ We note that the spectra of PEG-GNRs with BSA differ much from those in RPMI. Therefore, BSA alone cannot be responsible for the modifications seen in RPMI.²³

Cytotoxicity and cell viability

PEG-GNRs did not significantly affect the cell viability and were not cytotoxic, with the exception of our smallest size class. In order to evaluate the cytotoxic effects of PEG-GNRs, we combined two quantitative colorimetric assays indicating both survival/growth and viability of cultured cells. The inhibition of

cell growth was assessed by the SRB test, which measures the total amount of proteins, and therefore the presence of cells, in the microtiter plates. Cell viability was analyzed by the MTT test, which quantifies the reduction of tetrazolium salts by metabolically active cells. MTT is the test of choice in many studies on particle toxicity, thus enabling a direct comparison with the available literature.³⁰ Furthermore, we evaluated the effect of an acute treatment with PEG-GNRs on cell membrane integrity. The combination of different tests is important because the biological activity of gold nanoparticles and its mechanisms of action remain largely unknown and the output of each individual test may be biased by the interference with the particles.

Cell growth inhibition. The cytotoxic effects of PEG-GNRs were evaluated against four tumor cell lines (HeLa, A2780/S, SKOV3 and IGROV-1) after 72 and 168 hours exposure (Table 1 and Figure 3). After 72 hours, 50% inhibitory cell growth thresholds (IC₅₀) were not reached at gold concentrations up to 100 μ M. However, at the highest concentration (100 μ M Au), some inhibition was observed. Such an effect varied among the different cell lines: lower in HeLa cells (range 2.5-7.9%) and higher in IGROV-1 cells (range 35.9-46.3%), but without a clear pattern to particle size. After 168 h exposure, the IC₅₀ threshold was not reached in HeLa and A2780/S cells. In this case, at 100 μ M Au, the inhibitory growth effects on HeLa and A2780/S cells ranged from 1.8 to 15.8% and from 17.7 to 29.3%, respectively with irrelevant dependence on particle size. A similar behaviour was also observed in SKOV3 cells treated with larger GNRs 9, 3 and 1: although IC₅₀ values were not reached, the inhibitory effect at 100 μ M Au was 29.4, 22.5 and 39.5% respectively. Conversely, smaller GNRs 1/3 and 1/9 gave IC₅₀ values of 77.5 and 53.7 μ M Au, respectively, indicating that in this cell line the cytotoxicity of PEG-GNRs seems to grow with miniaturization. All PEG-GNRs exhibited IC₅₀ thresholds ranging from 10.3 to 41.0 μ M Au against IGROV-1 cells with poor dependence on particle size.

Cell viability. The effects of PEG-GNRs on cell viability were evaluated against four tumor cell lines (HeLa, A2780/S, SKOV3 and IGROV-1) after 24 hours exposure (Figure 4). All PEG-GNRs did not affect HeLa cells up to 100 μ M Au and exhibited a moderate inhibition of cell viability only at 300 μ M Au, which did not vary with particle size. A2780/s and IGROV-1 cells suffered from moderate inhibition of cell viability with all particle sizes, but this effect started at lower concentrations (10 μ M Au) for smaller GNRs 1/9 with respect to the others (30-100 μ M Au). The same trend was observed for SKOV3 cells. Although a different sensitivity of the various cell lines was observed, with HeLa cells holding the greatest resistance, the principal trends with particle size did not depend on cell line. Smaller particles provided slightly more MTT reduction inhibition, which falls below statistical relevance and emerged only at high gold concentrations.

Membrane integrity. Membrane stability after exposure to PEG-GNRs was assessed by fluorescence analysis of calcein efflux. Calcein-AM is a non fluorescent dye that permeates cell membranes. In live cells, intracellular esterase converts calcein-AM to green fluorescent calcein, which is unable to pass intact cell membranes. In the case of membrane integrity disruption,

Table 2 PEG-GNRs uptake by HeLa and J774a.1 cells after different incubation times. Data are referred to the same number of cells.

PEG-GNRs	Au (ng / 10 ⁶ cells)			
	J774a.1	HeLa		
	24 h	72 h	168 h	
9	462	1178	3001	1885
3	340	/	/	/
1	209	312	1218	974
1/3	272	/	/	/
1/9	865	80	341	292

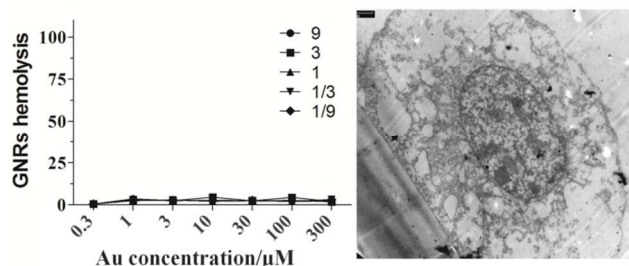


Fig. 6 Left: red blood cells haemolysis from PEG-GNRs of different average size: data represent a mean of two independent experiments, both performed in triplicate, and haemolysis values are expressed as percentage of positive control. Right: representative transmission electron micrograph displaying a J774a.1 cell cultured on a transwell membrane and treated with PEG-GNRs 1.

which may reflect multiple conditions of cell damage, a decrease in intracellular calcein fluorescence would be observed.⁵⁰ Figure 5 shows fluorescence images of A2780/s cells preloaded with calcein-AM and treated with PEG-GNRs. After 3h exposure at 300 μM Au, none of the particles induced leakage of calcein, thus indicating the absence of membrane permeabilization. All cell lines gave similar results (Figure S5 of the ESI).

Blood compatibility and cellular uptake

PEG-GNRs proved to be safe for intravenous injection, without haemolytic activity nor significant detection from immune cells, especially for smaller sizes. The potential of PEG-GNRs for biomedical applications depends on their compatibility with a systemic administration. In addition, their unspecific cellular uptake may impair their potential to reach specific targets such as tumors. We analyzed the effect of particle size on their haemolysis and unspecific uptake by HeLa cells taken as a standard model (Table 2). Moreover, we compared the results obtained with HeLa cells with a monocyte/macrophagic cell line (J774a.1), so as to distinguish the contribution of specific macrophage functions.

As indicated in Figure 6A, none of the particles showed haemolytic activity, even at the highest concentrations. Data are referred to positive controls obtained by dosing ultrapure water to induce complete haemolysis.

The effect of size on the cellular uptake of PEG-GNRs was investigated for three size classes with negligible statistical overlap (i.e. samples 1/9, 1 and 9, see Figure 1). The amount of gold internalized by HeLa cells exposed to 100 μM Au was evaluated at different time points. As shown in Table 2, there occurs little uptake in all samples, as it is expected for PEGylated particles and in particular GNRs.²⁰ As a rule of thumb, uptake

grows with particle size. Table 2 also reports the values obtained with J774a.1 cells after 24 hours of incubation and shows that both smaller and bigger PEG-GNRs are internalized to a bigger extent than those of an intermediate size.

The impact of PEG-GNRs on macrophages was also addressed by the analysis of TEM images of J774a.1 cells treated with sample 1 and prepared with a method that is most representative of the living structure. In figure 6B, the cell morphology clearly shows the absence of alterations. No particles were detected within the cell nucleus or cytoplasm but in sporadic endocytic vesicles, indicating the rarity of unspecific internalization.

Discussion

In this article, we have analyzed PEG-GNRs of different size classes, which fall in a range suitable for biomedical applications of principal interest such as photoacoustic imaging and optical hyperthermia of cancer. All PEG-GNRs are stable in PBS and their size does not modulate their interaction with proteins, which is very weak as it is seen in the case of cyt c. The data obtained with BSA are of particular relevance when considering PEG-GNRs for intravenous injection, albumin being the most abundant protein in the plasma. Conversely, the cell medium RPMI causes a significant red-shift of the plasmonic bands of all PEG-GNRs, although without evident precipitation. We hypothesize that different components of RPMI may cooperate to modify the microenvironment of the particles, inducing a partial substitution of their PEG portion and protein adsorption. However, the extent of red-shift that we observed does not preclude the particle capacity to interact with light. We note that PEG-GNRs can be suspended in PBS without flocculation nor visible optical changes for a few weeks at room temperature, which is compatible with the implementation of complex biological experiments.

In another set of experiments, we studied the cytotoxic effects of PEG-GNRs on four tumor cell lines. Inhibitory growth effects occurred only at the highest gold concentrations and after prolonged exposures, as long as one week, when structural modifications such as those seen in RPMI may intervene. Available literature data are limited to shorter exposures (i.e. 24 or 48 hours).^{51,52} A modulation of the cytotoxic effects in four cell lines suggests that the sensitivity to PEG-GNRs varies from model to model and is especially low for HeLa cells. Although HeLa cells are the most popular choice to compare the cytotoxicity of particles with different size and surface chemistry,⁵³ our evidence indicates that the inspection of additional cell lines and longer exposures can unveil new effects. The cytotoxicity observed at high concentrations and long incubation times may reflect the presence of contaminants on the particle surface, such as cetrimonium and silver.⁵⁴ While the identification of cetrimonium fell below our detection capabilities, we were able to assess the relative amount of silver by elemental analysis (Figure S6 of the ESI). This measurement confirmed that the silver content is higher for smaller particles, which reflects their larger specific surface area. We recall that, in HeLa cells, the trend of cellular uptake with particle size is opposite to the weak one observed for growth inhibition. In combination with the lack of plasmatic membrane permeabilization, these data refute any simple correlation between particle contact and cytotoxicity, which is more likely to

depend on the release of silver ions and other contaminants retained on the particle surface. In other words, the higher content of contaminants in smaller PEG-GNRs seems to over counteract the effect of a lower cellular uptake in the final cytotoxicity. An accurate quantification of the release of cetrinonium and silver ions into the cellular media will be the focus of our future efforts. We note that, according to Figure S6 of the ESI, a suspension containing 100 μM Au also comprises a total content of silver ranging between 0.6 – 1.6 ppm only, which is in the order of the sensitivity of our elemental analysis. The resultant release of silver ions falls below our current detection limits.

In the last set of experiments we considered two parameters that are crucial for the use of PEG-GNRs in biomedical applications requiring their intravenous administration. Alkilany et al. reported that blood vessels are not damaged by an exposure to PEG-GNRs.⁵⁵ Here, we demonstrated the absence of haemolysis and rarity of unspecific cellular uptake of PEG-GNRs. The latter grows with particle size. Previous studies reported a higher uptake for smaller particles.^{18,24,31} However those studies extended the range of particle sizes much below our GNRs 1/9, which we did not take into consideration because of their poor plasmonic behaviour and lack of synthetic methods. Other studies reported that the uptake of gold nanospheres displays a maximum for radii around 25 nm (see ref 21 and references therein). Our PEG-GNRs with equivalent radii ranging from 4.8 to 19.4 nm seem to fit in the positive slope of that curve, even though the comparison of spherical and cylindrical particles requires some caution.²⁰ These considerations hold for those cells that do not exhibit specific phagocytic functions or conditions such as our HeLa cells. We also considered a macrophagic cell line, in order to model the uptake that may follow from systemic administration by the mononuclear phagocyte system. In this case, we found a different trend for smaller particles, which is ascribed to a phagocytic activity.

Conclusions

In conclusion, PEG-GNRs are a stable platform for applications in biomedical optics. Their shape governs the frequency of their plasmonic resonances. Instead their size can be engineered to optimize the interface with an optical excitation and a biological environment for specific uses. Here we focused on the relationships between particle size and some biological profiles.

Modest PEG-GNRs cytotoxicity appears only at concentrations above 100 μM Au and after several days of incubation. This toxicity does not vary much with particle size. However some differences may arise from the larger specific surface area of smaller particles, which we associate with some contamination originating from the particle synthesis. Acute effects, such as membrane permeabilization and haemolysis, were not observed for any particle size. Data are coherent within different cell lines and toxicity tests, even though some models and parameters are more sensitive than others. Future efforts should focus on the removal of contaminants from PEG-GNRs without destabilizing the PEG coating.

The cellular uptake of PEG-GNRs is low and displays some modulation with particle size. Larger particles (say 85 nm length by 21 nm diameter) may be convenient for those contexts that require unspecific uptake, such as for loading of cellular

vehicles,^{56,57} while average particles (say 41 nm length by 10 nm diameter) may be ideal to inhibit unspecific uptake and pursue slower blood clearance or specificity by the addition of ligands. All this evidence, together with the absence of interactions with albumin, which is the most abundant protein in the plasma, suggests that PEG-GNRs are compatible with blood injection.

In essence, particle size does not overturn the safety and blood compatibility of PEGylated gold nanorods in their range of greatest biomedical interest, but may still provide alternatives for a fine modulation of functional biological profiles.

Acknowledgments

This work has been partially supported by the Projects of the Health Board of the Tuscan Region “NANOTREAT” and “NANO-CHROM”. We gratefully acknowledge Chiara Gabbiani for her work in the first stage of the project and Francesco Rugi for the ICP-AES measurements.

Notes and references

- ^a Institute of Applied Physics “Nello Carrara”, National Research Council, Via Madonna del Piano 10, Sesto Fiorentino, 50019 (Italy). Fax: +39 055 5226201; Tel: +39 055 5225307; E-mail: f.ratto@ifac.cnr.it
- ^b Dept. of Experimental and Clinical Medicine, University of Florence, Viale G. Pieraccini 6, Firenze, 50139 (Italy)
- ^c Dept. of Chemistry “Ugo Schiff”, University of Florence, Via della Lastruccia 3, Sesto Fiorentino, 50019 (Italy)
- ^d Dept. of Experimental and Clinical Biomedical Sciences, University of Florence, Viale G. Pieraccini 6, Firenze 50139 (Italy)
- † Electronic Supplementary Information (ESI) available: supplementary methods on cell lines and culture conditions, cell growth inhibition studies and cell viability studies; supplementary data on stability of PEGylated gold nanorods with lysozyme, stability of PEGylated gold nanorods with cyt c, interaction of PEGylated gold nanorods with cyt c, stability of PEGylated gold nanorods in RPMI, membrane integrity and particle composition by elemental analysis. See DOI: 10.1039/b000000x/
1. K. Huang, P.K. Jain, I.H. El-Sayed and M.A. El-Sayed, *Nanomedicine*, 2007, **2**, 681-93.
2. X. Huang, P.K. Jain, I.H. El-Sayed and M.A. El-Sayed, *Lasers Med. Sci.*, 2008, **23**, 217-28.
3. L. Tong, Q. Wei, A. Wie and J.X. Cheng, *Photochem. Photobiol.*, 2009, **85**, 21-32.
4. I.H. El-Sayed, *Curr. Oncol. Rep.*, 2010, **12**, 121-8.
5. F. Ratto, P. Matteini, S. Centi, F. Rossi and R. Pini, *J. Biophotonics*, 2011, **4**, 64-73.
6. A.M. Alkilany and C.J. Murphy, *J. Nanopart. Res.*, 2010, **12**, 2313-33.
7. N. Khlebtsov and L. Dykman, *Chem. Soc. Rev.*, 2011, **40**, 1647-71.
8. F. Ratto, P. Matteini, A. Cini, S. Centi, F. Rossi, F. Fusi and R. Pini, *J. Nanopart. Res.*, 2011, **13**, 4337-48.
9. J. Perez-Juste, I. Pastoriza-Santos, L.M. Liz-Marzan and P. Mulvaney, *Coordination Chem. Rev.*, 2005, **249**, 1870-901.
10. P.K. Jain, K.S. Lee, I.H. El-Sayed and M.A. El-Sayed, *J. Phys. Chem. B*, 2006, **110**, 7238-48.
11. P.K. Jain and M.A. El-Sayed, *Chem. Phys. Lett.*, 2010, **487**, 153-64.
12. A. Kopwithaya, K.T. Yong, R. Hu, I. Roy, H. Ding, L.A. Vathy, E.J. Bergey and P.N. Prasad, *Nanotechnology*, 2010, **21**, 315101.
13. R.G. Rayavarapu, W. Petersen, L. Hartsuiker, P. Chin, H. Janssen, F.W. van Leeuwen, C. Otto, S. Manohar and T.G. van Leeuwen, *Nanotechnology*, 2010, **21**, 145101.
14. C. Grabinski, N. Schaeublin, A. Wijaya, H. D' Couto, S.H. Baxamusa, K. Hamad-Schifferli and S.M. Hussain, *ACS Nano*, 2011, **5**, 2870-9.
15. T. Mironava, M. Hadjiargyrou, M. Simon, V. Jurukovski and M.H. Rafailovich, *Nanotoxicology*, 2010, **4**, 120-37.

16. C. Freese, M.I. Gibson, H.A. Klok, R.E. Unger and C.J. Kirkpatrick, *Biomacromolecules*, 2012, **13**, 1533-43.
17. E. Oh, J.B. Delehanty, K.E. Sapsford, K. Susumu, R. Goswami, J.B. Blanco-Canosa, P.E. Dawson, J. Granek, M. Shoff, Q. Zhang, P.L. Goering, A. Huston and I.L. Medintz, *ACS Nano*, 2011, **5**, 6434-48.
18. X.D. Zhang, D. Wu, X. Shen, P.X. Liu, N. Yang, B. Zhao, H. Zhang, Y.M. Sun, L.A. Zhang and F.Y. Fan, *Int. J. Nanomedicine*, 2011, **6**, 2071-81.
19. P. Matteini, F. Ratto, F. Rossi and R. Pini, *J. Biomed. Opt.*, 2012, **17**, 010701.
20. B.D. Chithrani, A.A. Ghazani, W.C. Chan, *Nano Lett.*, 2006, **6**, 662-8.
21. C.D. Walkey, J.B. Olsen, H. Guo, A. Emili and W.C. Chan, *J. Am. Chem. Soc.*, 2012, **134**, 2139-47.
22. S. Chakraborty, P. Joshi, V. Shanker, Z.A. Ansari, S.P. Singh and P. Chakrabarti, *Langmuir*, 2011, **27**, 7722-31.
23. W.S. Cho, S. Kim, B.S. Han, W.C. Son and J. Jeong, *Toxicol. Lett.*, 2009, **191**, 96-102.
24. M.A. Abdelhalim, *Lipids Health Dis.*, 2011, **10**, 205.
25. L.S. Rieznicchenko, S.M. Dybkova, T.G. Gruzina, Z.R. Ulberg, I.N. Todor, N.Y. Lukyanova, S.I. Shpyleva and V.F. Chekhun, *Exp. Oncol.*, 2012, **34**, 25-8.
26. M. Schulz, L. Ma-Hock, S. Brill, V. Strauss, S. Treumann, S. Gröters, B. van Ravenzwaay and R. Landsiedel, *Mutat. Res.*, 2012, **745**, 51-7.
27. G. Vecchio, A. Galeone, V. Brunetti, G. Maiorano, S. Sabella, R. Cingolani and P.P. Pompa, *PLoS One*, 2012, **7**, e29980.
28. T. Niidome, M. Yamagata, Y. Okamoto, Y. Akiyama, H. Takahashi, T. Kawano, Y. Katayama and Y. Niidome, *J. Control. Release*, 2006, **114**, 343-7.
29. I.P. Lau, H. Chen, J. Wang, H.C. Ong, K.G. Leung, H.P. Ho, and S.K. Kong, *Nanotoxicology*, 2011, **6**, 847-56.
30. A.M. Alkilany, L.B. Thompson, S.P. Boulous, P.N. Sisco and C.J. Murphy, *Adv. Drug. Deliv. Rev.*, 2012, **64**, 190-9.
31. W.S. Cho, M. Cho, J. Jeong, M. Choi, H.Y. Cho, B.S. Han, S.H. Kim, H.O. Kim, Y.T. Lim, B.H. Chung and J. Jeong, *Toxicol. Appl. Pharmacol.*, 2009, **236**, 16-24.
32. E.B. Dickerson, E.C. Dreaden, X. Huang, I.H. El-Sayed, H. Chu, S. Pushpanketh, J.F. McDonald and M.A. El-Sayed, *Cancer Lett.*, 2008, **269**, 57-66.
33. G. von Maltzahn, J.H. Park, A. Agrawal, N.K. Bandaru, S.K. Das, M.J. Sailor and S.N. Bhatia, *Cancer Res.*, 2009, **69**, 3892-900;
34. W.I. Choi, J.Y. Kim, C. Kang, C.C. Byeon, Y.H. Kim and G. Tae, *ACS Nano*, 2011, **5**, 1995-2003
35. A.F. Bagley, S. Hill, G.S. Rogers and S.N. Bhatia, *ACS Nano*, 2013, **7**, 8089-97.
36. F. Ratto, P. Matteini, F. Rossi and R. Pini, *J. Nanopart. Res.* 2010, **12**, 2029-36.
37. L. Cavigli, M. de Angelis, F. Ratto, P. Matteini, F. Rossi, S. Centi, F. Fusi and R. Pini, *J. Phys. Chem. C*, 2014, DOI: 10.1021/jp502647p.
38. P. Skekan, R. Stroeang, D. Scudiero, A. Monks, J. McMahon, D. Vistica, J.T. Warren, H. Bokesch, S. Kenney and M.R. Boyd, *J. Natl. Cancer Inst.*, 1990, **82**, 1107-12.
39. T. Mosmann, *J. Immunol. Methods*, 1983, **65**, 55-63.
40. E. Fantechi, G. Campo, D. Carta, A. Corrias, C. de Julián Fernández, D. Gatteschi, C. Innocenti, F. Pineider, F. Ruggi and C. Sangregorio, *J. Phys. Chem. C*, 2012, **116**, 8261-70.
41. B. Nikoobakht and M.A. El-Sayed, *Chem. Mater.*, 2003, **15**, 1957-62.
42. R. Mercatelli, G. Romano, F. Ratto, P. Matteini, S. Centi, F. Cialdai, M. Monici, R. Pini and F. Fusi, *Appl. Phys. Lett.*, 2011, **99**, 131113.
43. X.D. Xu and M.B. Cortie, *Adv. Funct. Mat.* 2006, **16**, 2170-6.
44. J.L. Perry, K.G. Reuter, M.P. Kai, K.P. Herlihy, S.W. Jones, J.C. Luft, M. Napier, J.E. Bear and J.M. DeSimone, *Nano Lett.* 2012, **12**, 5304-10
45. S. Link and M.A. El Sayed, *Int. Rev. Phys. Chem.*, 2000, **19**, 409-53.
46. G.S. Terentyuk, G.N. Maslyakova, L.V. Suleymanova, B.N. Khlebtsov, B.Y. Kogan, G.G. Akchurin, A.V. Shantrocha, I.L. Maksimova, N.G. Khlebtsov and V.V. Tuchin, *J. Biophotonics*, 2009, **2**, 292-302.
47. M. Iosin, F. Toderas, P.L. Baldeck, S. Astilean, *J. Mol. Struct.*, 2009, **196**, 924-6.
48. K. Saha, A. Bajaj, B. Duncan and V.M. Rotello, *Small*, 2011, **7**, 1903-18.
49. C. Li, C. Wu, J. Zheng, J. Lai, C. Zhang and Y. Zhao, *Langmuir*, 2010, **26**, 9130-5.
50. J.C. Bischof, J. Padanilam, W.H. Holmes, R.M. Ezzell, R.C. Lee, R.G. Tompkins, M.L. Yarmush and M. Toner, *Biophys. J.*, 1995, **68**, 2608-14.
51. M. Mahmood, D.A. Casciano, T. Mocan, C. Iancu, Y. Xu, L. Mocan, D.T. Iancu, E. Dervishi, Z. Li, M. Abdalmuhsen, A.R. Biris, N. Ali, P. Howard and A.S. Biris, *J. Appl. Toxicol.*, 2010, **30**, 74-83.
52. W. Cui, J. Li, Y. Zhang, H. Rong, W. Lu and L. Jiang, *Nanomedicine*, 2012, **8**, 46-53.
53. Y. Pan, S. Neuss, A. Leifert, M. Fischler, F. Wen, U. Simon, G. Schmid, W. Brandau and W. Jahnen-Dechent, *Small*, 2007, **3**, 1941-9.
54. A.M. Alkilany, P.N. Nagaria, C.R. Hexel, T.J. Shaw, C.J. Murphy and M.D. Wyatt, *Small*, 2009, **5**, 701-8.
55. A.M. Alkilany, A. Shatanawi, T. Kurtz, R.B. Caldwell and R.W. Caldwell, *Small*, 2012, **8**, 1270-8.
56. S.K. Baek, A.R. Makkouk, T. Krasieva, C.H. Sun, S.J. Madsen and H. Hirschberg, *J. Neurooncol.*, 2011, **104**, 439-48.
57. S.J. Madsen, S.K. Baek, A.R. Makkouk, T. Krasieva and H. Hirschberg, *Ann. Biomed. Eng.*, 2012, **40**, 507-15.